JOURNAL OF PROPULSION AND POWER
Vol. 20, No. 2, March–April 2004

Methane Dissociation in Pulsed dc Discharges at High Reduced Electric Field

S. Douglas Marcum*
Miami University, Oxford, Ohio 45056
and
John W. Parish† and Biswa N. Ganguly‡
U.S. Air Force Research Laboratory, Wright–Patterson Air Force Base, Ohio 45433

High-speed discharge imaging, current/voltage characteristic, and time-resolved emission spectroscopic measurements were performed on fast-rise (20 ns), short-pulsed (400 ns), high-voltage (4–8 kV) dc discharges into CH_4 and pure H_2 flows at 50 torr as functions of discharge gap (0.25–1.00 cm). Additionally, the discharges were spectrally imaged using plasma emissions from the C_2 bands near 516 nm and the CH band at 431 nm. The dependence of discharge homogeneity on discharge gap at constant pressure and discharge gas preionization are documented. Current/voltage measurements with variable gap give a sheath voltage drop of 300 V and an average *E/N* of 80 Townsends during the steady-state portion of the discharges, and up to 300 Td during the early part of the discharge pulse (5-kV drive voltage). Under conditions that enhance discharge inhomogeneity, C_2 emissions are substantially brighter (∼factor of 7) than when the discharge is diffuse. This suggests that the buildup of carbon clusters on the discharge electrodes plays a role in the formation of highly inhomogeneous discharge geometries. Time-resolved measurements of H_α radiation in CH_4 and H_2 discharges suggest significant H-atom production (∼10^{14} H atoms/cm^3) during a single discharge pulse into CH_4 with 5.6-mJ (0.70-mJ/cm^3) pulse energy.

Nomenclature

A_{32}, A_{3j}	=	Einstein coefficient for spontaneous emission for the indicated transition
C	=	constant containing all detection system optical and geometrical parameters
$[CH_4]$	=	number density of methane
D_e	=	energy required for dissociation
d	=	discharge gap
E	=	electric field magnitude
E/N	=	reduced electric field measured in Townsends (Td) (note: 1 Td $= 10^{-17}$ V cm$^2 = 0.323$ V/Torr cm at 300 K)
$E_{\text{th}}^{\text{gas}}(D)$	=	threshold for dissociation of a given discharge gas
$E_{\text{th}}^{\text{gas}}(DE)$	=	threshold for dissociative excitation to H($n = 3$) for a given discharge gas
$[H]_{\text{gas}}$	=	number density of H atoms in a given discharge gas
$[H_2]$	=	number density of molecular hydrogen
$h\nu_{32}$	=	photon energy for H($n = 3$ to 2) or H_α emission
$I_{\text{H}\alpha}^{\text{gas}}$	=	intensity of H_α emission from a given discharge gas
k_e^{gas}	=	electron impact dissociative excitation rate coefficient
$k_{\text{ei}}^{\text{gas}}$	=	rate coefficient for electron impact excitation to H($n = 3$) for a given discharge gas
k_Q^{gas}	=	quenching coefficient for H($n = 3$) atoms in a given gas
N	=	gas number density
n	=	principal quantum number
n_e^{gas}	=	electron density in a given discharge gas
P_{gas}	=	discharge power deposited into a given gas
p	=	pressure
t	=	time
V	=	discharge volume
$X(E/N)$	=	fraction of discharge power deposited into dissociation as a function of E/N
$XY(\text{state label}^{\text{multiplicity}}\Lambda_{\text{parity}})$	=	generic molecular electronic state designation
$Y(E/N)$, $Y'(E/N)$	=	fraction of discharge power deposited into direct electron impact excitation as a function of E/N
Δv	=	change in vibrational quantum number

Subscripts and Superscripts

gas	=	hydrogen or methane

Received 12 November 2002; revision received 10 June 2003; accepted for publication 7 July 2003.

*Associate Professor, Department of Physics. Member AIAA.
†Research Associate, National Research Council.
‡Principal Research Physicist. Associate Fellow AIAA.

Introduction

ATOMIC hydrogen, hydrocarbon fragments, and their radicals are important species for initiating ignition and sustaining stable flame propagation. Molecular gas discharges generally give rise to a complex set of interactions between atoms, internally excited molecules, and radicals. Globally, discharge power is deposited via inelastic electron collisions into molecular species as rotational, vibrational, or electronic excitation and via dissociation or ionization. Clearly the various channels compete for discharge energy, with the fractional power transferred to each being a strong function of E/N (where E is the electric field and N is the gas density). At low

E/N rotational and vibrational excitation typically dominates. As the discharge E/N is increased, dissociation, electronic excitation, and ionization collectively share the bulk of the input discharge power.[1,2] Highly nonequilibrium plasma production of energetic reactive hydrocarbon fragments could have application in situations where more conventional means of promoting and sustaining combustion are degraded.

One such situation is found in supersonic combustion ramjet (scramjet) propulsion systems where the flow speed is so high that mixing and reaction times are limited.[3–6] Some flow conditions also give rise to very low mixture temperatures.[3] For either condition additional sources of ignition or combustion enhancement are needed. Plasma torch ignitors[3] have been investigated widely, and microwave discharges[5] have been studied, both as means of providing reliable scramjet combustion. However, such approaches require multikilowatt electrical power inputs and are not easily volume scaleable.

The efficacy of the plasma torch approach is attributed to the introduction of atomic hydrogen[3] into the flow because the reaction $H + O_2 -> OH + O$ is an important chain branching reaction[7,8] for combustion [rate constant (Ref. 9) $= 2.65 \times 10^{+16} T^{-0.671}$ $e^{-(17041\ cal/mol)/RT}$ cm^3/mol s]. A plasma torch, typically using a flowing Ar-H_2 mixture, operates at low E/N and high T, and acts to thermally dissociate hydrogen in a low E/N arc discharge. Hence the energy requirement is high. Pulsed dc glow discharges with high E/N in pure H_2 and H_2-N_2 mixtures[1,2] have demonstrated efficient direct electron impact dissociation of hydrogen with substantially lower power requirements. The attractiveness of high E/N pulsed discharges for fostering dissociation, electronic excitation, and ionization is clear. Pulsed dc discharges in gaseous hydrocarbon mixtures similarly provide substantial atomic hydrogen, as well as electronically excited hydrocarbon fragment neutrals and ions. Evidence of dissociative excitation of methane in such discharges producing fast H atoms near the cathode sheath with kinetic energies up to an electron volt (or T ~ 11,000 K) has been reported.[10] Such discharge products would be useful in promoting combustion in a wide variety of fuel-to-air mixtures. Additionally, control of discharge parameters offers the possibility of varying the yields of the dominant reaction products in response to changing conditions in an application.

Discharges in methane and methane-bearing mixtures have been the focus of a number of recent studies with a variety of potential applications. For example, pulsed discharges in methane have been shown to provide efficient conversion to acetylene and hydrogen.[11,12] Similar discharges have been employed for plasma carburizing of surfaces[13] and for the production carbon-based nanoparticles.[14,15]

The primary goals of this study were to 1) construct a discharge system capable of producing uniform methane discharges over a substantial range of high E/N values and 2) conduct imaging and spectroscopic measurements of the resulting plasma emissions sufficient to document plasma uniformity and provide an estimate of H-atom production. Pulsed gas discharges in CH_4 produce all possible methane fragments (CH_3, CH_2, CH, C, and H) and their ions in varying ratios depending upon the discharge E/N. Additionally, some carbon clustering occurs.[13–15] Of these, excited neutrals of atomic hydrogen, CH, and C_2 were chosen for spectroscopic observation because of their easily detected visible emissions [H_α at 656 nm, the CH ($A^2\Delta - X^2\Pi$) band at 431 nm, and the $C_2(A^3\Pi_g - X^3\Pi_u, \Delta v = 0)$ Swan bands near 516 nm (Refs. 16 and 17)]. Comparison of H_α emissions in the CH_4 discharges with that of the much better characterized H_2 discharges[1,2,18–20] provides the desired H-atom production estimate. The correlation of bright C_2-band emission with discharge inhomogeneity is also documented and discussed. The issue of discharge homogeneity might be important for determination of scaling parameters such as energy density per pulse as the streamer dimension changes with pressure.

Experimental Details

A schematic diagram of the experimental apparatus is shown in Fig. 1. The main components of the apparatus are the discharge cell,

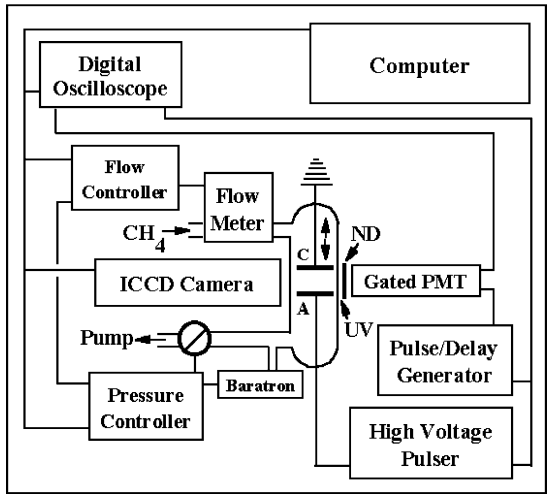

Fig. 1 Schematic diagram of the experimental apparatus.

the light detection electronics, and the high-voltage pulser. The discharge cell was a cylindrical glass enclosure, approximately 37 cm in height and 7.5 cm in diameter. Two sets of opposed fused silica windows (5-cm diam), orthogonal to each other, were available as viewports. The cell was evacuated through 3.5-cm i.d. glass and metal lines by a roughing pump. The base pressure for the cell was 3 mtorr.

The discharge gas flow was metered by flow controllers (MKS Type 1259 flow controller and a MKS Type 247C four-channel readout), while the cell pressure was governed by a control valve and an exhaust valve controller (MKS Types 253A and 252, respectively). The gas pressure was measured with a baratron pressure gauge (MKS Type 102A) whose output was sent to the valve controller to maintain constant pressure in the discharge cell. The gas flow could be varied between 0–100 standard cubic centimeters per minute (SCCM), and the baratron operated in the pressure range 0–100 torr. Gas pressure and flow rate were set by input to the PC. Throughout this study the gas flow rate was fixed at 30 SCCM and the pressure p at 50 torr. Discharge gases were UHP grade (99.999%).

The discharge electrodes were two aluminum discs 3.2 cm in diameter with an interelectrode spacing d that varied between 0.25–1.0 cm in this work [pressure-gap product (pd) product range 12.5–50 torr cm]. The discharge pulse repetition rate used was 10 Hz throughout. The interelectrode space could be illuminated by an UV preionization lamp. The high-voltage pulser constructed for this study powered the discharge and is based upon a stacked MOSFET switch. Output current/ voltage measurements were made using high-voltage probes (HP Model P6015) across the discharge and across a series current sense resistor. The probe outputs were monitored by a digital oscilloscope (LeCroy 9354C) for both single-shot signal capture and averaging (100 shots). Current and voltage waveforms were then transferred to a PC for processing.

High-speed direct-discharge imaging and spectral imaging were done using a gateable, intensified CCD camera (Princeton Instruments Model ICCD-576). Spectral images were made using 10-nm bandpass filters at 431 nm (CH) and 516 nm (C_2). Time-resolved H_α, CH, or C_2 emissions from the discharge were detected using a gated photomultiplier tube (PMT; Hamamatsu R1477). Light was collected through an iris diaphragm by a focusing lens and passed through the appropriate bandpass filter onto the PMT. The PMT was under a constant bias throughout the experiment and was gated on for a 5-μs period encompassing the discharge pulse duration. Neutral density filters were used to avoid saturation. The PMT output was sent to a digital oscilloscope for signal capture and averaging (100 shots) and to a PC as already stated. Single-shot emission profiles were also recorded, which in no case deviated significantly from profiles measured by averaging at 10 Hz. This was expected because no significant buildup of discharge fragments from pulse to pulse could occur as a result of the low dissociation fraction (<0.001) per pulse, the low repetition rate used, and the gas flow conditions employed. When discharge imaging is not being conducted, a second

gated PMT in place of the camera allows for simultaneous time-resolved emission spectroscopy of a pair of methane fragments.

Results and Discussion

Discharge Characterization

Averaged current, gap voltage, and power waveforms for discharges in pure methane at 50 torr and using a 5-kV pulser drive voltage are shown in Fig. 2 for four different electrode spacings (1.0, 0.75, 0.50, and 0.25 cm). The pulser provides rapid excitation pulse rise and fall times (typically <20 ns), control over pulse duration, and low jitter (typically <10 ns). Note that the discharge current turns on earlier as the gap is decreased. A fixed trigger pulse width of 440 ns was used throughout this work.

The current pulse rise is typically delayed relative to that of the gap voltage pulse by roughly 25 ns in each case, and there is a substantial overlap between current and voltage during the short initial peak in the voltage pulse. The power curves reflect the degree of overlap with the brief [~30 ns full width at half maximum (FWHM)], high-power initial peak that occurs at each gap. Additionally, no indications of arc formation are seen by way of sudden voltage drops and associated current excursions; pulse-to-pulse shape variations are minimal.

In all cases the gap voltage falls to a lower steady-state value after the initial peak until the pulser is triggered off. This implies that discharge E/N is substantially higher during the initial pulse peak than in the relatively long final steady-state period. To determine E/N from the gap voltage and the discharge conditions (50 torr, 300 K), the voltage drop across the thin (~50 μm) cathode sheath must subtracted. The sheath drop and average E/N for the discharges were estimated during the steady-state portion by plotting the average voltage (between 200–400 ns) against electrode separation, as shown in Fig. 3. Though pd varies by a factor of four, the data bear the usual linear relationship[21–23] and indicate reasonable values for both the sheath drop of 300 V and an average E/N of 80 Td. When that sheath voltage drop is subtracted from the measured gap voltages, shown in Fig. 2, average E/N during the steady-state portion of the discharges agrees well with that value. E/N conditions during the initial breakdown portion of the discharge pulses range up to a factor of four higher than the steady-state portion of the pulse.

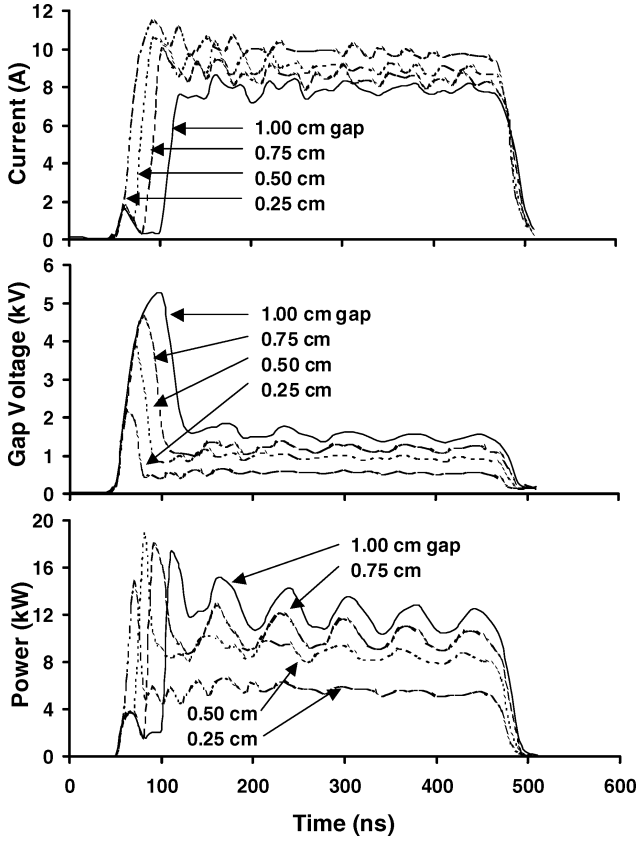

Fig. 2 Current, gap voltage, and power characteristics for discharges into 50 torr CH_4 and 5-kV pulser drive voltage as functions of discharge gap.

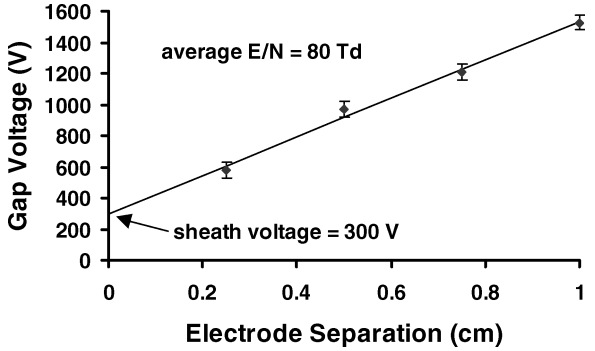

Fig. 3 Average gap voltage between 200–400 ns plotted against anode–cathode gap (see Fig. 2).

The range of E/N values found here is attractive from the viewpoint of assessing the hydrocarbon fragment yield as a function of E/N. To determine if the discharge can also be made sufficiently diffuse to facilitate fragment yield measurements by laser spectroscopy techniques, discharge imaging, spectral imaging, and time-resolved spectroscopy techniques were used. Because of the short duration of a typical discharge pulse, the discharges were imaged with a gateable, intensified CCD camera to determine the degree of homogeneity and pulse-to-pulse variability.

Discharge V-I pulse shapes, especially rise times, and discharge pd values are important determinants of discharge uniformity,[21–23] as are levels and methods of discharge gas preionization.[24] Using discharge conditions identical to those shown in Figs. 2 and 3, Fig. 4 shows typical 100-ns exposures documenting the effect that decreasing the electrode spacing has upon discharge uniformity. The transition between multiple streamer discharge and diffuse discharge occurs under the indicated conditions between 0.5- and 0.25-cm gaps or below a pressure–discharge gap product (pd) of 25 torr-cm.

The behavior of the discharge as a function of pulser drive voltage is shown in Fig. 5 for a fixed gap of 1.0 cm and drive voltages of 4, 6, and 8 kV. All other experimental parameters are identical to those just discussed. Features here are similar to those of Fig. 2, except that the current rise time and turn on time are much slower for the lowest drive voltage. Here too the gap voltage pulses peak just before the corresponding current turns on, the degree of overlap being reflected in the corresponding power curves. The overvoltage at the beginning of the pulse is clearly most effective for power deposition at high E/N conditions.

Extracting the temporal evolution of discharge E/N from the preceding gap voltage pulses was accomplished by subtracting the sheath voltage drop from the gap voltage and accounting for discharge conditions (300 K, 50 torr, 1-cm gap). This procedure is valid because sheath voltage develops within a few nanoseconds of the onset of the current rise.[25] (Time is inversely proportional to the plasma electron frequency.) The result is shown in Fig. 6. Again note the overlap with the corresponding current pulses: the high E/N values early on for the 4-kV drive voltage is largely ineffective given the late turn on time for that case. However, the high peak power for the higher drive voltages substantially overlaps the early high E/N values, a result that is a major determinant of time resolved hydrocarbon fragment emission profiles.

Time-resolved H_α- and CH-band emissions (431 nm) for experimental conditions identical to those shown in the preceding two figures are shown in Fig. 7. The effect of direct electron impact excited methane fragment [H($n=3$) and CH($A^2\Delta$) states] production of the early high E/N values for the higher drive voltages is clear, though the emission profiles and relative intensities are somewhat different. Both emissions rise at the same rate as the discharge power pulse, indicating direct electron impact dissociative excitation of methane as their sources. The brighter (factor of five) CH

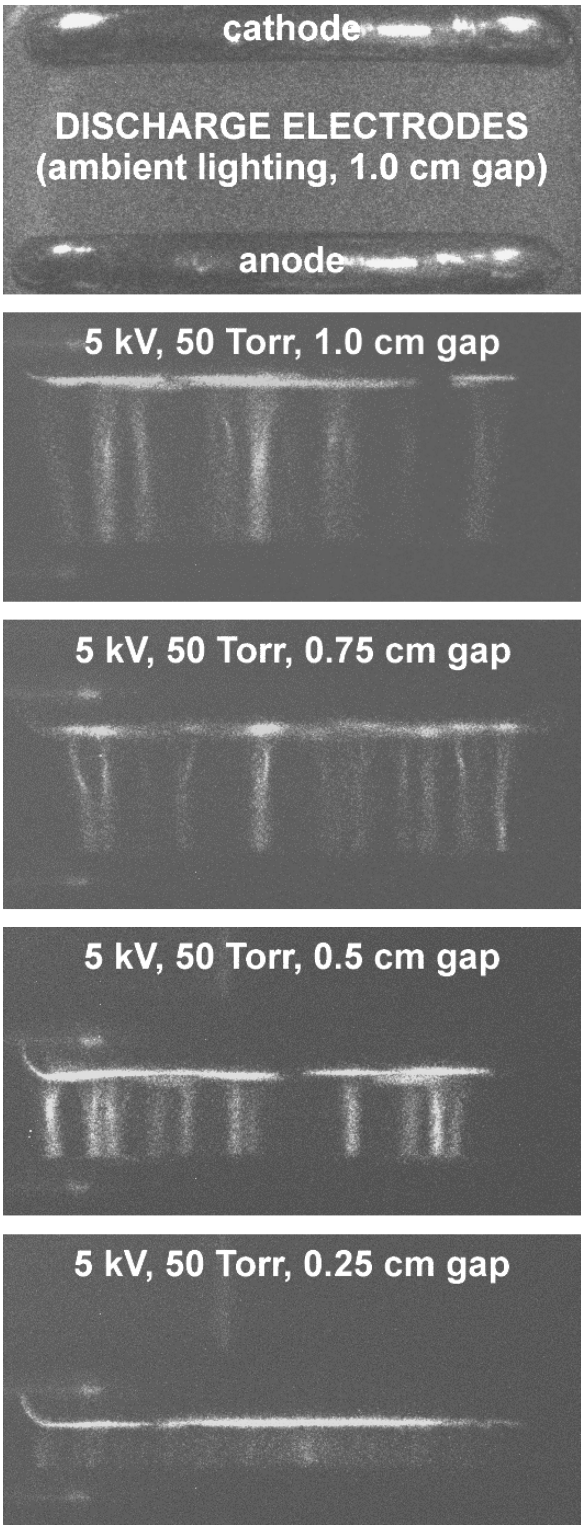

Fig. 4 Direct, high-speed two-dimensional CH_4 discharge emission images as a function of interelectrode spacing.

emission has a markedly long fall time because of the long radiative lifetime and the low quenching[26] rate compared to very strongly quenched[27–29] H($n = 3$) atomic level. At 50 torr the H_α emission profile very closely resembles that of the discharge power for all drive voltages. For the higher drive voltages there is a short current peak at the beginning of the pulses. However, both the H_α and CH emissions are much more significantly enhanced at the beginning of the pulse than current pulse shapes would suggest, thus showing the effect on methane fragmentation that results from the high E/N conditions early on.

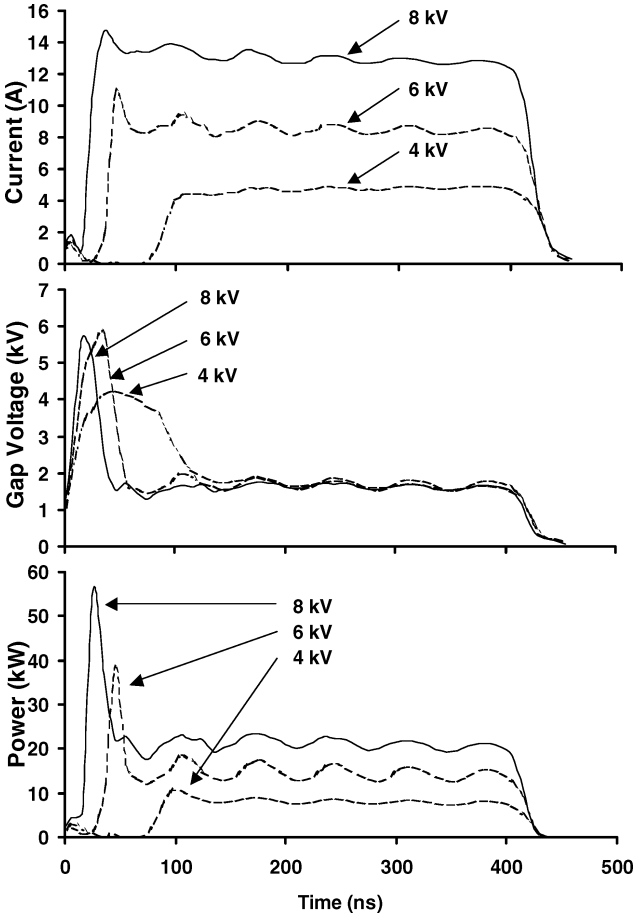

Fig. 5 Current, gap voltage, and power characteristics as functions of pulser drive voltage for discharges into 50 torr CH_4 and a 1.0-cm electrode gap.

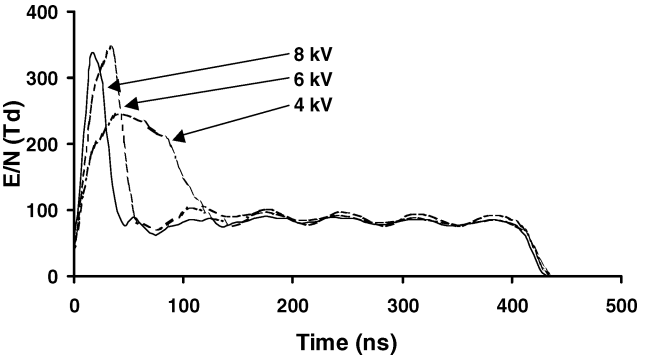

Fig. 6 Temporal evolution of the discharge *E/N* for three drive voltages, a 1-cm gap, and 50 torr methane.

The final time-resolved emission results from CH_4 discharges reported here are for the C_2 Swan bands[16,17] near 516 nm. Complemented by discharge imaging and spectral imaging of the C_2 and CH bands, the rare occurrence of highly inhomogeneous discharges can be partially understood. On rare occasions discharge images indicated the presence of only one or two very bright streamers in the discharge. Almost entirely absent at the smallest gap studied, the incidence of such highly inhomogeneous discharge pulses grew to roughly 3% of pulses at the largest gap of 1.0 cm. Further, a dramatic increase in bright streamer formation frequency occurred in the absence of irradiation of the discharge space by the UV preionization source. Insights into a potential cause of the formation of a few bright streamers as opposed to multiple streamer discharges were suggested by related ongoing investigations.[10] Vibrationally hot C_2 bands have been observed in similar discharges, and at higher

pressures (100 torr) visible carbon deposits have been observed to form on the discharge electrodes.

Figure 8 shows five single-shot current pulses and their corresponding $C_2(A^3\Pi_g - X^3\Pi_u,\ \Delta v = 0)$ emission profiles (near 516 nm), taken with and without UV preionization of the discharge. Images of those same pulses are shown in Fig. 9. The discharge conditions were 0.75-cm discharge gap, 50 torr methane, and drive voltage of 5 kV. Except for a delayed single shot in the case without UV irradiation, the current pulses are essentially identical between the two cases, and clearly quite repeatable. The clearest difference between the two data sets is the much greater brightness without UV irradiation. Inspection of Fig. 9 correlates the bright streamer discharge conditions with bright C_2 emission. The rise of the more typical diffuse and weak emissions in the case with UV irradiation essentially follows the current.

Clearly, the discharge fully dissociates some fraction of methane, and some carbon atoms subsequently combine to form C_2 and presumably larger carbon clusters. The brighter emission and different temporal emission profile suggest the possible involvement of large carbon clusters breaking up under direct electron impact within the gap or being detached from the cathode and breaking up as the pulse rises. Carbon clusters that formed during repetitive pulsing of the discharge could adhere to the electrodes providing both the source of the bright streamers as well as the vibrationally hot C_2 bands.[10] Such processes would locally enhance the discharge conductivity and contribute to the formation of inhomogeneous plasmas with one or two bright streamers. The C_2 emission profiles in the case of highly inhomogeneous bright streamer discharges are different from any other observed emission profile (see Fig. 7), suggesting different kinetics involved in excitation of the C_2 molecule in those cases.

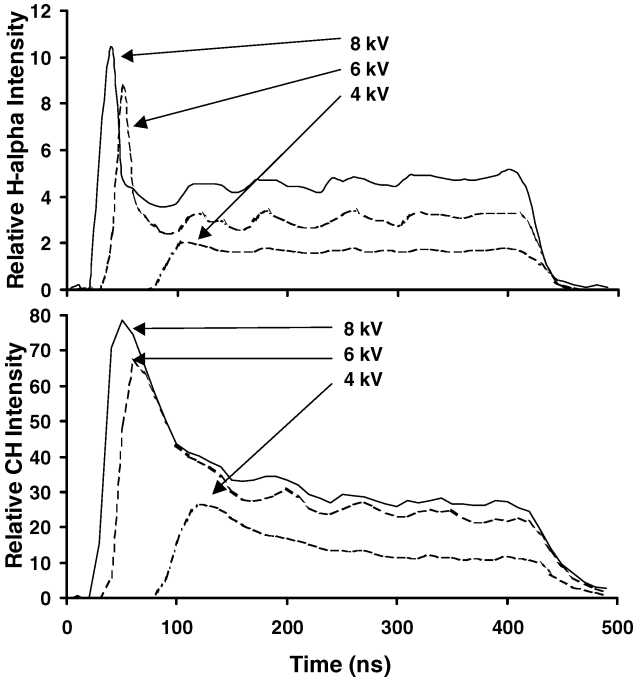

Fig. 7 Temporal evolution of the most intense visible emissions from the excited hydrocarbon fragments: H_α and CH (431-nm band). The H_α emission essentially follows the discharge power pulse, whereas the CH emission peak occurs later in time. Experimental conditions are the same as for Figs. 5 and 6.

The final experimental results associated with the discharge characterization show the spatial distribution of C_2 emissions in comparison with that of the brightest hydrocarbon fragment emission bands of CH. Figure 10 shows images of the discharges similar to those of Fig. 9, except that they have been imaged through bandpass (10-nm FWHM) filters. The typical spatial distribution of the C_2 emission is quite uniform and weak (upper left) when the discharge is diffuse, indicating a largely uniform distribution of C_2. Bright streamer formation is clearly accompanied by strongly enhanced C_2 emission (upper right). The spatial distribution of the CH emission is quite similar to that of C_2 regardless of the degree of discharge homogeneity.

H-atom Production

Using the technique of actinometry,[30–33] an estimate of H-atom production during a discharge pulse can be made by comparing the H_α emission from the methane discharge (Fig. 7) to that from the very well-characterized pure H_2 discharge[1,2,18–20] under the same experimental conditions. Gap voltage, discharge power, and the resulting H_α emission from discharges into pure hydrogen at 50 torr using a 6-kV pulser drive voltage are shown in Fig. 11. The temporal behavior of the gap voltage and discharge power are very similar to the analogous case for discharges into methane (see Fig. 5, 6-kV drive voltage case), although both fall more rapidly in the hydrogen plasma during the latter portion of the discharge pulse. This behavior clearly indicates that discharge E/N in the pure hydrogen discharges decreases somewhat more during the latter portion of the discharge pulse, as opposed to remaining essentially constant after the initial high E/N peak in methane (see Fig. 6, 6-kV case). The likely cause of the minor difference in temporal behavior is that the methane plasmas are slightly electronegative. The H_α emission from the pure hydrogen discharge shown in Fig. 11 follows the discharge power pulse, identical to the temporal behavior of the H_α emission from methane (compare to Fig. 7, 6-kV case).

Discharges in pure hydrogen have been extensively studied,[1,2,18–20] and the fraction of the discharge power deposited into the various inelastic modes of hydrogen as a function of E/N has been established. For E/N above 80 Td, the fraction of the discharge

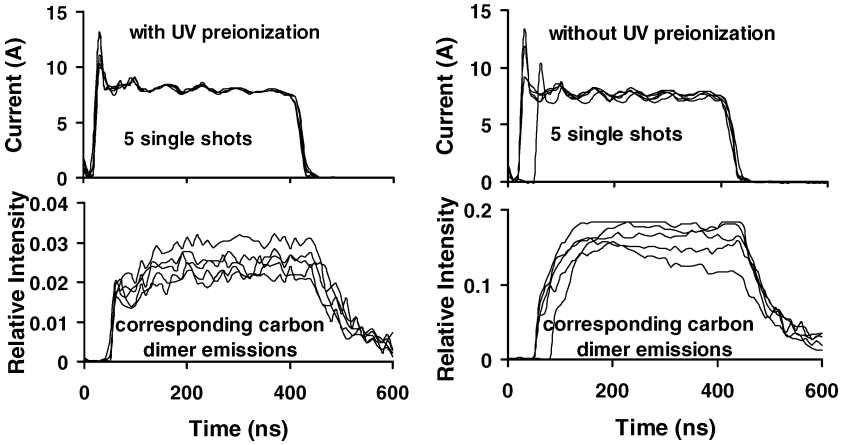

Fig. 8 Single-shot current pulses and the corresponding C_2 Swan-band emission profiles near 516 nm for cases with and without UV irradiation of the discharge gas. Discharge conditions are 50 torr methane, 5-kV drive voltage, and fixed gap of 0.75 cm. The corresponding direct discharge images are presented in Fig. 10.

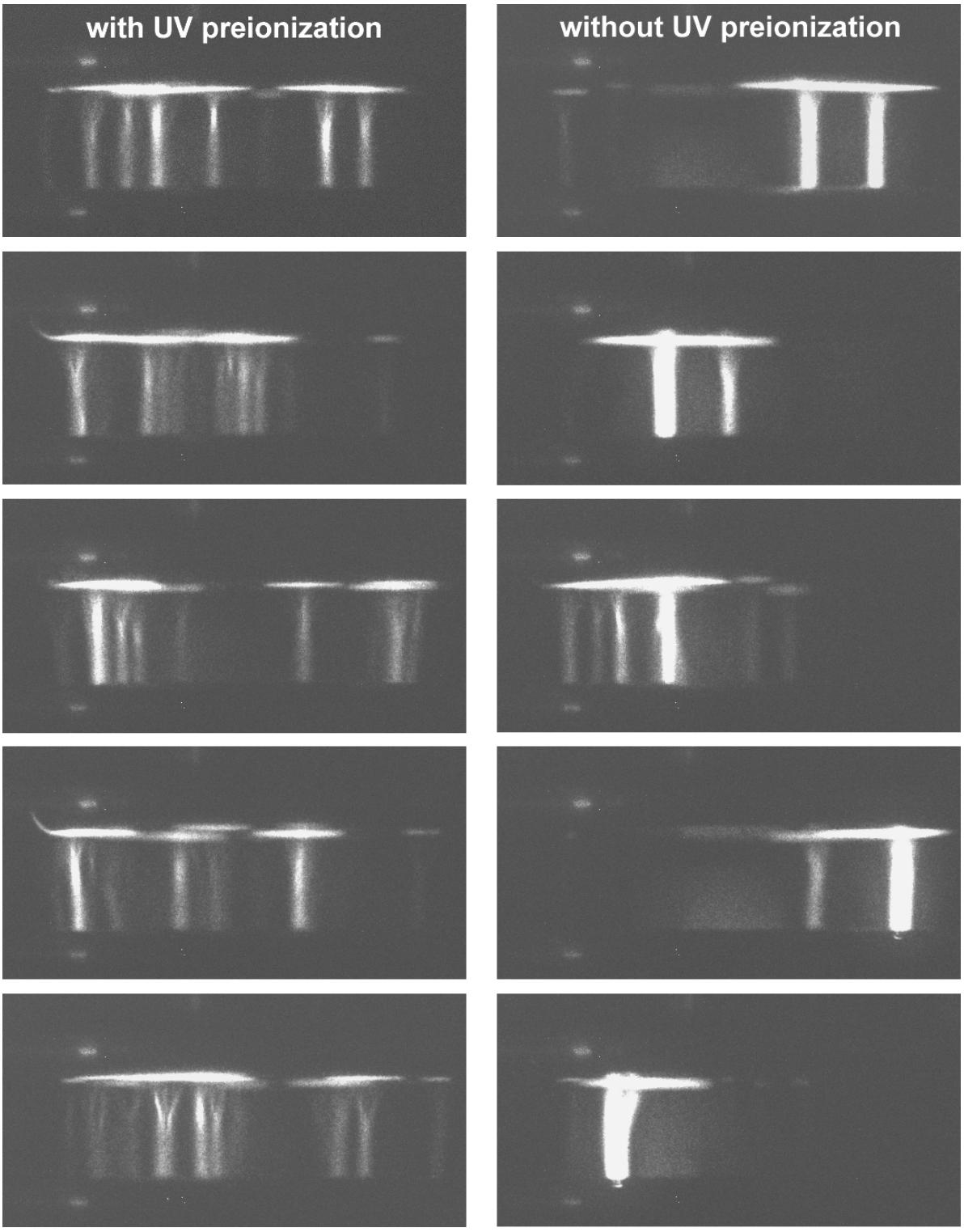

Fig. 9 Direct-discharge images of the same discharge pulses shown in Fig. 10, with UV-irradiated discharges on the left. Bright streamer formation is much more common when the discharge gas is not preionized.

power producing dissociation[2] of H_2 into two H atoms is greater than 50%. Absolute H-atom density and H_α-emission measurements[1] for such discharges have also been made as a function of discharge E/N. Thus, it is possible to write the number density of H atoms produced in pure hydrogen discharges as

$$[\mathrm{H}]_{\mathrm{H2}} = \frac{2\int X(E/N)P_{\mathrm{H2}}\,\mathrm{d}t}{D_e V} \tag{1}$$

where P_{H2} is discharge power and D_e is the electron impact dissociation energy of H_2 (9.8 eV). The factor of two accounts for the fact that each dissociation event produces two hydrogen atoms. Equation (1) can be used to directly determine the H-atom production in short-pulsed pure-hydrogen discharges from electrical measurements alone because the only volume destruction mechanism is the three-body reaction $H + H + H_2 -> 2H_2$ [rate constant (Ref. 34) $= 9.0 \times 10^{16}\ T^{-0.6}$ cm^6/mol^2 s], which is negligibly slow under the experimental conditions used.

H_α emission from such a discharge results from the competition between production of H($n = 3$) atoms, and losses by radiation, or by collisional quenching, to the ground state. As just noted, the rapid rise of H_α emission (in concert with the rise in the discharge power)

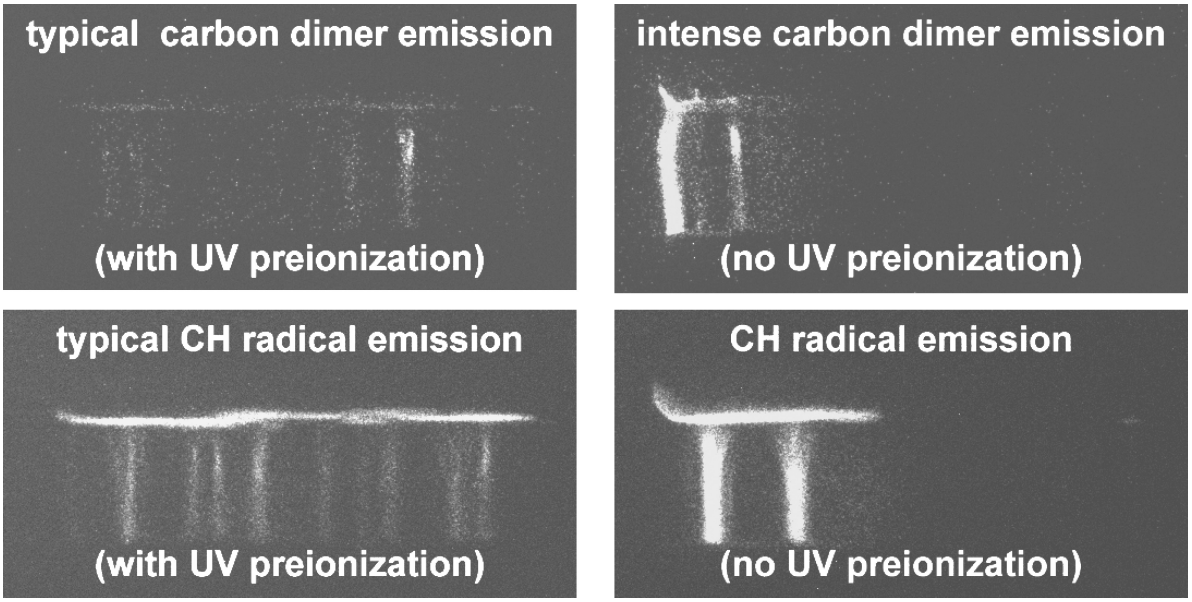

Fig. 10 Spatial distribution of C_2 and CH emissions for typical discharges (left) and highly inhomogeneous bright streamer discharges (right).

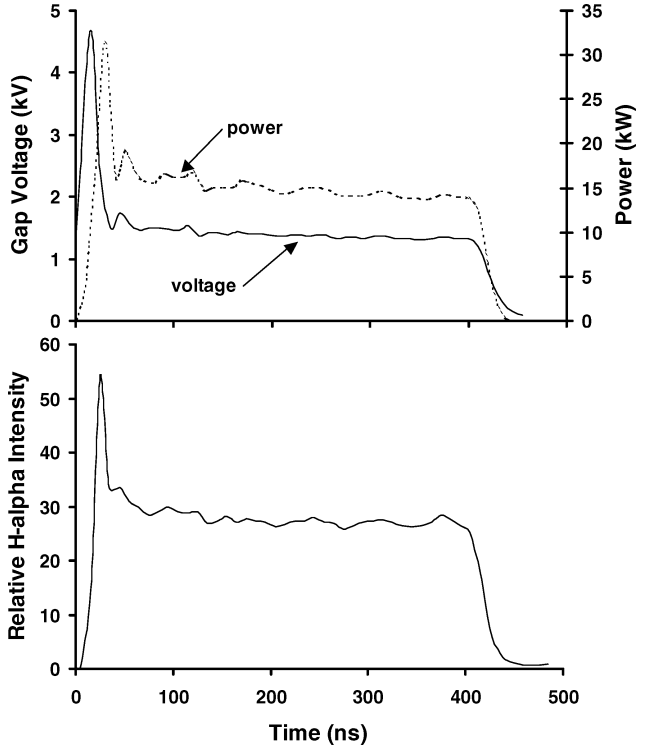

Fig. 11 Current and gap voltage characteristics (top) and the resulting H_α emission (bottom) for discharges into pure H_2 at 50 torr pressure, 1.0-cm gap, and a drive voltage of 6 kV (each area 100 shot averages). Compare to Figs. 5 and 7 for CH_4 discharges.

indicates that production of H($n=3$) atoms in this study proceeds by direct electron impact dissociative excitation of the parent gas. The resulting H_α emission intensity can be written[30–33] as the ratio of the rate of production to that of loss:

$$I_{H\alpha}^{H2} = \frac{Ch\nu_{32}A_{32}k_e^{H2}n_e^{H2}[H_2]}{\sum_j A_{3j} + k_Q^{H2}[H_2]} \tag{2}$$

Here n_e^{H2} is the electron density in the hydrogen discharge and ΣA_{ij} is the sum of the A coefficients for all radiative deexcitation processes from the H($n=3$) level (H_α and Lyman$_\beta$). The coefficients k_e^{H2} and k_Q^{H2} quantify electron impact dissociative excitation of H_2 to H($n=3$) + H(1 s) and the quenching rate of H($n=3$) atoms in hydrogen, respectively. The square brackets denote number density.

For discharges into pure CH_4, the resulting H_α emission intensity can similarly be written as

$$I_{H\alpha}^{CH4} = \frac{Ch\nu_{32}A_{32}k_e^{CH4}n_e^{CH4}[CH_4]}{\sum_j A_{3j} + k_Q^{CH4}[CH_4]} \tag{3}$$

where the symbols have analogous meanings. The main reaction that consumes atomic hydrogen is $H + CH_4 -> CH_3 + H_2$ [rate constant (Ref. 35) $= 6.6 \times 10^8\ T^{1.62}e^{-(10840\ cal/mol)/RT}\ cm^3/mol\ s$]. Here too, reactions with the background gas that would remove H atoms are insignificant and therefore can be neglected under the experimental conditions employed. Thus, the ratio of H_α emissions from the two discharges is simply

$$\frac{I_{H\alpha}^{H2}}{I_{H\alpha}^{CH4}} = \frac{k_e^{H2}n_e^{H2}[H_2]}{k_e^{CH4}n_e^{CH4}[CH_4]} \frac{\sum_j A_{3j} + k_Q^{CH4}[CH_4]}{\sum_j A_{3j} + k_Q^{H2}[H_2]} \tag{4}$$

It has been shown that H-atom production in pulsed discharges in hydrogen (measured by two-photon-allowed laser-induced fluorescence) is directly proportional to the H_α emission signal.[1] The same relation between H-atom production and H_α emission should hold for

$$\left[E_{th}^{H2}(DE) = 19\ \text{eV}, \quad E_{th}^{CH4}(DE) = 20\ \text{eV},\right.$$

$$\left.\text{and} \quad E_{th}^{H2}(D) = 9.8\ \text{eV}, \quad E_{th}^{CH4}(D) = 8.8\ eV\right]$$

discharges in methane because the thresholds for both electron impact dissociative excitation[36,37] (DE) and dissociation[36,38] (D) are nearly the same in both hydrogen and methane. Further, the energy dependencies of the relevant cross sections near theshold for both dissociative excitation and dissociation of hydrogen and methane are quite similar.[36,38] The threshold for direct electron impact excitation of H atoms to H($n=3$) is, of course, independent of the parent gas. Together, these facts allow substitution of the ratio of production rates of H($n=3$) atoms by dissociative excitation in Eq. (4) with the corresponding rates of direct electron impact excitation of ground-state H atoms to the H($n=3$) level because the rates of those processes are proportional. With that substitution Eq. (4) becomes

$$\frac{I_{H\alpha}^{H2}}{I_{H\alpha}^{CH4}} = \frac{k_{ei}^{H2}n_e^{H2}[H]_{H2}}{k_{ei}^{CH4}n_e^{CH4}[H]_{CH4}} \frac{\sum_j A_{3j} + k_Q^{CH4}[CH_4]}{\sum_j A_{3j} + k_Q^{H2}[H_2]} \tag{5}$$

where the subscript ei indicates the rate coefficient for electron impact excitation of H atoms to H($n=3$) and $[H]_{H2}$ and $[H]_{CH4}$ refer to the number density of H atoms in the hydrogen and methane discharges, respectively.

The product of the direct electron impact excitation rate coefficient and electron density in each plasma is proportional to the fraction of discharge power devoted to that process multiplied by the power deposited in the gas, that is,

$$k_{ei}^{H2} n_e^{H2} \propto Y(E/N) P_{H2}, \qquad k_{ei}^{CH4} n_e^{CH4} \propto Y'(E/N) P_{CH4} \quad (6)$$

where $Y(E/N)$ is the known[2] fractional power deposited into electron impact production of H($n=3$) as a function of E/N in hydrogen and $Y'(E/N)$ is the analogous factor in methane discharges. Note that the proportionality constants in Eq. (6) are the inverse of the excitation potential of H($n=3$) and are therefore identical for each of those relations. Substitution of Eqs. (1) and (6) into Eq. (5) and taking $Y = Y'$(because the rates are identical), the final expression used to estimate H-atom production in the CH_4 discharges of interest can be written as

$$[H]_{CH4} \approx \frac{I_{H\alpha}^{CH4}}{I_{H\alpha}^{H2}} \frac{P_{H2}}{P_{CH4}} \frac{\sum_j A_{3j} + k_Q^{CH4}[CH_4]}{\sum_j A_{3j} + k_Q^{H}[H_2]} \frac{2\int X(E/N) P_{H2}\, dt}{D_e V} \quad (7)$$

In this relation the relevant quenching rate constants for H($n=3$) atoms[26–29] are 2×10^{-9} cm^3/s in H_2 and 3.5×10^{-9} cm^3/s in CH_4, and the measured H_α intensity profiles needed as inputs are shown in Figs. 7 (6-kV drive voltage case) and 11 for emission from methane and hydrogen discharges, respectively. The discharge power profiles are shown in Fig. 5 for methane (6-kV drive voltage case) and Fig. 11 for hydrogen. The factor X was taken to be 0.6 during the initial high E/N peak in the power pulse and 0.45 during the much longer steady-state portion of the discharge (see Figs. 6 and 11).

Using Eq. (1), the H-atom production during a single discharge pulse into 50 torr of pure hydrogen using a pulser drive voltage of 6 kV was calculated and is shown as the upper plot in Fig. 12. Similarly, using Eq. (7), the H-atom production during a single discharge pulse into methane under the same experimental conditions is shown in the lower plot of that figure. For comparison purposes the discharge pulse power and the associated H_α emission are also shown in that plot. Note that the production rate is significantly higher during the brief high E/N early peak in the discharge pulse that is typical in such fast discharges. Production of $\approx 2 \times 10^{14}$ H atoms per cubic centimeter of discharge volume during a 400-ns discharge pulse is significant. The total energy deposited in the gas during a pulse is 5.6 mJ, and the energy deposited per unit volume is 0.7 mJ/cm^3. Verification of that level of H-atom production will require the use of two-photon laser-induced fluorescence or mass spectrometric measurements of CH_4 fragments.

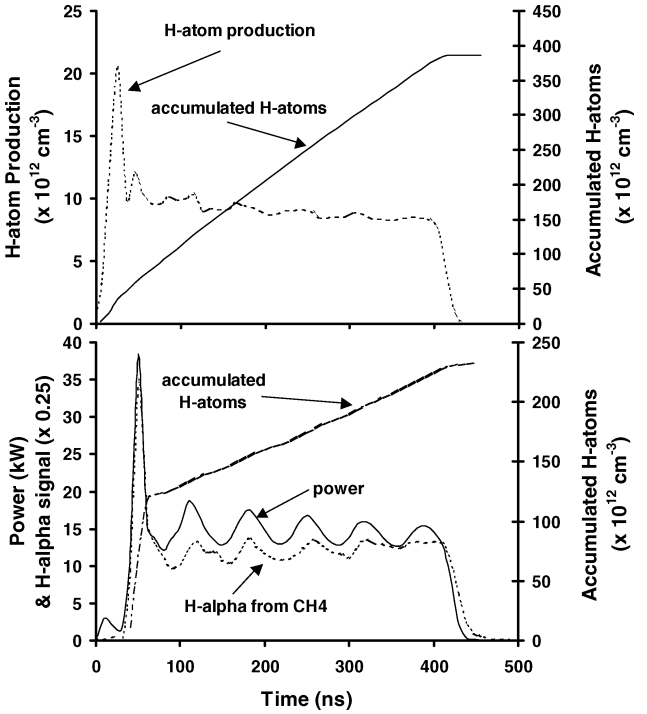

Fig. 12 Estimated H-atom production in pure hydrogen (top) and methane (bottom), each during a discharge pulse. Both are determined from experiments using a 1-cm gap, a pulser drive voltage of 6 kV, and 50 torr gas pressure.

Summary

Techniques for the control of the transition from diffuse to inhomogeneous plasmas in high E/N hydrocarbon discharges have been established. The steady-state portion of the discharge voltage pulse follows the classic pd scaling[21–23] relationship over the pd range studied (12.5–50 torr cm). The resulting plasmas are typically diffuse in the lower end of that pd range, and even at the higher pd values are sufficiently uniform (multiple streamers).

Significant levels of hydrogen-atom production by fast, high E/N discharges are estimated from the measured H_α emission profiles and by the application of an actinometric model. The results are quite encouraging from the viewpoint of application to scramjet ignition and combustion sustainment.

Acknowledgment

S. D. Marcum acknowledges the support of the National Research Council under the Summer Faculty Fellowship Program.

References

[1]Williamson, J. M., and Ganguly, B. N., "Hydrogen Dissociation in a H_2-N_2 Pulsed DC Glow Discharge," *Physical Review E*, Vol. 61, No. 5, 2000, pp. 5734–5752.

[2]Nagpal, R., Ganguly, B. N., Bletzinger, P., and Garscadden, A., "Power Deposition in H_2 and H_2-N Glow Discharges," *Chemical Physics Letters*, Vol. 257, No. 3, 1996, pp. 386–392.

[3]Wagner, T. C., O'Brien, W. F., Northam, G. B., and Eggers, J. M., "Plasma Torch Ignitor for Scramjets," *Journal of Propulsion and Power*, Vol. 5, No. 5, 1989, pp. 548–554.

[4]Mitani, T., "Ignition Problems in Scramjet Testing," *Combustion and Flame*, Vol. 101, No. 3, 1995, pp. 347–359.

[5]Khodataev, K., and Ershov, A., "Experimental Investigation of a Possibility of a MW Streamer Gas Discharge Application for Furle Ignition in a Jet Engine," *Proceedings of the 2nd Weekly Ionized Gases Workshop, Supplement*, AIAA, Reston, VA, 1998, pp. 339–350 (unpublished).

[6]Buriko, Y. Y., Vinogradov, V. A., Goltsev, V. F., and Waltrup, P. J., "Influence of Radical Concentration and Fuel Decomposition on Ignition of Propane/Air Mixture," *Journal of Propulsion and Power*, Vol. 18, No. 5, 2002, pp. 1049–1060.

[7]Roth, P., and Just, T. H., "Kinetics of the High Temperature, Low Concentration CH_4 Oxidation Verified by H and O Atom Measurements," *Proceedings of the 20th Symposium (International) on Combustion*, Combustion Inst., 1984, pp. 807–818.

[8]Briko, Y. Y., Vinogradov, V. A., Goltsev, V. F., and Waltrup, P., "Influence of Radical Concentration on Ignition of Propane/Air Mixture," *Journal of Propulsion and Power*, Vol. 18, No. 5, 2002, pp. 1049–1058.

[9]Yu, C.-L., Frenklach, M., Masten, D. A., Hanson, C. T., and Bowman, C. T., "Reexamination Shock-Tube Measurements of the Rate Coefficient of $H + O_2 -> OH + O$," *Journal of Physical Chemistry*, Vol. 98, No. 17, 1994, pp. 4770, 4771.

[10]Brown, M., and Ganguly, B., "Dissociation of CH_4 in Pulsed DC Discharges with Implications for Low-Temperature Ignition Chemistry," AIAA Paper 2003-0702, Jan. 2003.

[11]Yao, S. L., Suzuki, E., and Nakayama, A., "The Pyrolysis Property of a Pulsed Plasma of Methane," *Plasma Chemistry and Plasma Processing*, Vol. 21, No. 4, 2001, pp. 651–663.

[12]Yao, S. L., Suzuki, E., Meng, N., and Nakayama, A., "A High-Efficiency Reactor for the Pulsed Plasma Conversion of Methane," *Plasma Chemistry and Plasma Processing*, Vol. 22, No. 2, 2002, pp. 225–237.

[13]Rie, K.-T., Menthe, E., and Woehle, J., "Optimization and Control of a Plasma Carburizing Process by Means of Optical Emission Spectroscopy," *Surface and Coating Technology*, Vol. 98, No. 1, 1998, pp. 1192–1198.

[14]Stoffels, W. W., Stoffels, E., Ceccone, G., and Rossi, F., "Laser-Induced Particle Formation and Coalescence in a Methane Discharge," *Journal of Vacuum Science and Technology A*, Vol. 17, No. 6, 1999, pp. 3385–3392.

[15]Geraud-Grenier, I., Massereau-Guilbaud, V., and Plain, A., "Particulate Growth in a 13.56 MHz Radiofrequency Methane Plasma: Influence of the Flow Rate and the Incident RF Power," *European Physical Journal, Applied Physics*, Vol. 14, No. 3, 2001, pp. 187–192.

[16]Herzberg, G., *Electronic Spectra of Polyatomic Molecules*, Van Nostrand, Princeton, NJ, 1966, pp. 31, 273.

[17]Gaydon, A. G., *The Spectroscopy of Flames*, Wiley, New York, 1974, pp. 144–146.

[18]Ganguly, B. N., and Bletzinger, P., "Comparison of Hydrogen Atom Density Measurements in Three Types of Discharges Using H_2-N_2 Gas Mixtures," *Journal of Applied Physics*, Vol. 82, No. 10, 1997, pp. 4772–4776.

[19]Bletzinger, P., and Ganguly, B. N., "High Fractional Dissociation Efficiency in H_2 and H_2-N_2 Gas Mixtures in a Helical Resonator Discharge," *Chemical Physics Letters*, Vol. 247, No. 4, 1995, pp. 584–588.

[20]Ganguly, B. N., and Bletzinger, P., "Fractional Dissociation Efficiency Measurements of D_2 in a Helical Resonator D_2-N_2 Gas Mixture Discharge," *Applied Physics Letters*, Vol. 72, No. 13, 1998, pp. 1570, 1571.

[21]Von Engel, A., *Ionized Gases*, American Inst. of Physics, New York, 1995, pp. 195–215.

[22]Nasser, E., *Fundamentals of Gaseous Ionization and Plasma Electronics*, Wiley, New York, 1971, pp. 245–248.

[23]Raizer, Y. P., *Gas Discharge Physics*, Springer-Verlag, New York, 1992, pp. 334–342.

[24]Beer, T. A., Laimer, J., and Stori, H., "Study of the Ignition Behavior of a Pulsed dc Discharge Used for Plasma-Assisted Chemical-Vapor Deposition," *Journal of Vacuum Science and Technology A*, Vol. 18, No. 2, 2000, pp. 423–434.

[25]Czarnetzki, U., Luggenholscher, D., and Dobele, H. F., "Investigations on Ionic Processes and Dynamics in the Sheath Region of Helium and Hydrogen Discharges by Laser Spectroscopic Electric Field Measurements," *Applied Physics A*, Vol. 72, No. 5, 2001, pp. 509–521.

[26]Cooper, J. L., and Whitehead, J. C., "Collisional Removal Rates for Electronically Excited CH Radicals $B^2\Sigma^-$ and $C^2\Sigma^+$," *Journal of the Chemical Society Faraday Transactions*, Vol. 88, No. 16, 1992, pp. 2323–2327.

[27]Glass-Maujean, M., Lauer, S., Liebel, H., and Schmoranzer, H., "Collisional Quenching of the H($n=3$) Atoms by Molecular Hydrogen: Cross Section Measurements," *Journal of Physics B*, Vol. 33, No. 21, 2000, pp. 4593–4601.

[28]Lauer, S., Liebel, H., Vollweiler, F., Wilhelmi, O., Kneip, R., Fleming, E., Schmoranzer, H., and Glass-Maujean, M., "Collisional Quenching of H(3l) Atoms by Molecular Hydrogen," *Journal of Physics B*, Vol. 31, No. 13, 1998, pp. 3049–3056.

[29]Bittner, J., Kohse-Hoinghaus, K., Meier, U., and Just, T., "Quenching of Two-Photon-Excited H(3s,3d) and O(3p $^3P_{2,1,0}$) Atoms by Rare Gases and Small Molecules," *Chemical Physics Letters*, Vol. 143, No. 6, 1988, pp. 571–576.

[30]Coburn, J. W., and Chen, M., "Optical Emission Spectroscopy of Reactive Plasmas: A Method for Correlating Emission Intensities to Reactive Particle Density," *Journal of Applied Physics*, Vol. 51, No. 6, 1980, pp. 3134–3136.

[31]Pagnon, D., Amorim, J., Nahorny, J., Touzeau, M., and Vialle, M., "On the Use of Actinometry to Measure the Dissociation in O_2 DC Glow Discharges: Determination of the Wall Recombination Probability," *Journal of Physics D (Applied Physics)*, Vol. 28, No. 9, 1995, pp. 1856–1868.

[32]Barshilia, H. C., and Vankar, V. D., "Concentration of Atomic Hydrogen in the Ground State in a CH_4-H_2 Microwave Plasma," *Journal of Applied Physics*, Vol. 80, No. 7, 1996, pp. 3694–3698.

[33]Katsch, H. M., Tewes, A., Quandt, E., Goehlich, A., Kawetzki, T., and Dobele, H. F., "Detection of Atomic Oxygen: Improvement of Actinometry and Comparison with Laser Spectroscopy," *Journal of Applied Physics*, Vol. 88, No. 11, 2000, pp. 6232–6238.

[34]Frenklach, M., Wang, H., and Rabinowitz, M. J., "Optimization and Analysis of Large Chemical Kinetic Mechanisms Using the Solution Mapping Method—Combustion of Methane," *Progress in Energy and Combustion Science*, Vol. 18, No. 1, 1992, pp. 47–73.

[35]Rabinowitz, M. J., Sutherland, J. W., Patterson, P. M., and Klemm, R. B., "Direct Rate Constant Measurements for $H + CH_4 -> CH_3 + H_2$, 897-1729 K Using the Flash Photolysis-Shock Tube Technique," *Journal of Physical Chemistry*, Vol. 95, No. 2, 1991, pp. 674–681.

[36]Janev, R. K., Langer, W. D., Evans, K., Jr., and Post, D. E., Jr., *Elementary Processes in Hydrogen-Helium Plasmas*, Springer-Verlag, New York, 1989, pp. 20, 44, 45, 50, 51.

[37]Motohashi, K., Soshi, H., Ukai, M., and Tsurubuchi, S., "Dissociative Excitation of CH_4 by Electron Impact: Emission Cross Sections for the Fragment Species," *Chemical Physics*, Vol. 213, No. 1, 1996, pp. 369–384.

[38]Janev, R. K., and Reiter, D., "Collision Processes of CH_y and CH_y^+ Hydrocarbons with Plasma Electrons and Protons," *Physics of Plasmas*, Vol. 9, No. 9, 2002, pp. 4071–4081.